Basal ganglia and cortical control of thalamic rebound spikes

Mohammadreza Mohagheghi Nejad[1,2], Stefan Rotter[1], Robert Schmidt[3]

[1]*Bernstein Center Freiburg & Faculty of Biology, University of Freiburg, 79104 Freiburg, Germany*
[2]*Department of Computational Science and Technology, School of Electrical Engineering and Computer Science, KTH Royal Institute of Technology, 100 44 Stockholm, Sweden*
[3]*Department of Psychology, University of Sheffield, S1 2LT Sheffield, United Kingdom*

Abbreviated title: Basal ganglia control of thalamic rebound spikes

Corresponding Author:
Mohammadreza M. Nejad, Bernstein Center Freiburg, University of Freiburg, Hansastrasse 9A, 79104 Freiburg, Germany. Email: m.mohaghegh@gmail.com

Number of pages: 49

Number of figures: 6

Number of tables: 1

Number of words Abstract: 232

Keywords (up to 5): Parkinson's disease, Higher-order correlations, Nigrothalamic transmission, Active decorrelation, Nigral sensory responses

Abstract

Basal ganglia output neurons transmit motor signals by decreasing their firing rate during movement. This decrease can lead to post-inhibitory rebound spikes in thalamocortical neurons in motor thalamus. While in healthy animals neural activity in the basal ganglia is markedly uncorrelated, in Parkinson's disease neural activity becomes pathologically correlated. Here we investigated the impact of correlations in the basal ganglia output on the transmission of motor signals to motor thalamus using a Hodgkin-Huxley model of a thalamocortical neuron. We found that correlations in the basal ganglia output disrupt the transmission of motor signals via rebound spikes by decreasing the signal-to-noise ratio and increasing the trial-to-trial variability. We further examined the role of brief sensory responses in basal ganglia output neurons and the effect of cortical excitation of motor thalamus in modulating rebound spiking. Interestingly, both the sensory responses and cortical inputs could either promote or suppress the generation of rebound spikes depending on their timing relative to the motor signal. Finally, in the model rebound spiking occurred despite the presence of moderate levels of excitation, indicating that rebound spiking might be feasible in a parameter regime relevant also in vivo. Overall, our model provides novel insights into the transmission of motor signals from the basal ganglia to motor thalamus by suggesting new functional roles for active decorrelation and sensory responses in the basal ganglia, as well as cortical excitation of motor thalamus.

Introduction

The basal ganglia have long been implicated in the selection and execution of voluntary movements (Albin et al., 1989; Alexander and Crutcher, 1990b; Redgrave et al., 1999; Hikosaka et al., 2000). Classic "box-and-arrow" models of the basal ganglia (Alexander and Crutcher, 1990a; Wichmann and DeLong, 1996) presume a propagation of motor signals through the direct pathway. The direct pathway consists of direct, inhibitory projections from the striatum to the basal ganglia output regions. Therefore increased activity in the striatum reduces the activity e.g. in the substantia nigra pars reticulata (SNr). SNr in turn disinhibits the motor thalamus (Deniau and Chevalier, 1985), and thereby enables movement. Basal ganglia output neurons often have high baseline firing rates and decrease their rate during movement in both rodents and primates (Hikosaka and Wurtz, 1983; Schultz, 1986; Leblois et al., 2007; Schmidt et al., 2013). However, recent studies have suggested a more complex picture on how basal ganglia output affects motor thalamus and motor cortex (Bosch-Bouju et al., 2013; Goldberg et al., 2013).

Three different modes have been proposed for how the basal ganglia output can affect thalamic targets (Goldberg et al., 2013). In the first mode sudden pauses in basal ganglia inhibition of thalamus lead to "rebound" spikes in thalamocortical neurons due to their intrinsic T-type Ca^{2+} channels (Llinás and Jahnsen, 1982). Release from long-lasting hyperpolarisation (e.g. during movement) de-inactivates the T-type Ca^{2+} channels and thereby depolarises the membrane potential. For strong enough preceding hyperpolarisation, the membrane potential can even reach the spike threshold without any excitation (Person and Perkel, 2005; Person and Perkel, 2007;

Leblois et al., 2009; Kim et al., 2017). However, thalamocortical neurons also receive excitatory input from cortex, which can change the effect of nigrothalamic inhibition. For moderate levels of cortical excitation the nigrothalamic transmission operates in a disinhibition mode, in which the basal ganglia effectively gate cortical excitation, so that during pauses of inhibition the excitatory inputs can evoke spikes in the thalamocortical neuron (Kojima and Doupe, 2009; Bosch-Bouju et al., 2014; Edgerton and Jaeger, 2014). If the cortical excitation is strong enough, the inhibition from the basal ganglia no longer prevents action potentials in the thalamocortical neurons, but instead controls their timing. In this "entrainment" mode the thalamocortical neuron spikes after the inhibitory input spikes from SNr with a short, fixed latency (Goldberg and Fee, 2012; Goldberg et al., 2012).

One prominent feature of the basal ganglia network is that neurons fire in an uncorrelated fashion, despite their overlapping dendritic fields and local recurrent connections (Wilson, 2013). Specific features of the basal ganglia such as pacemaking neurons and high firing rate heterogeneity may act as mechanisms for active decorrelation of activity. This effectively prevents correlations among neurons, and disrupting this mechanism leads to pathologically correlated activity as in Parkinson's disease (Bar-Gad et al., 2003; Wilson, 2013). Increased correlated activity has also been observed in basal ganglia output neurons in Parkinson's disease (Bergman et al., 1998), which can in turn increase correlated activity in the thalamus (Reitsma et al., 2011). Previous computational modelling has shown that pathological basal ganglia output can prevent the thalamic relaying of cortical excitatory signals (Guo et al., 2008). Here we examined how pathological correlations

in the basal ganglia output affect the transmission of motor signals from the basal ganglia to the thalamus and how this transmission is affected by cortical excitation. In addition to transmitting motor signals, basal ganglia output neurons may also be involved in further sensory and cognitive processing. For example, SNr neurons also respond to salient sensory stimuli instructing the initiation or stopping of movements (Pan et al., 2013; Schmidt et al., 2013). Therefore, we also investigated how these sensory responses may affect the motor transmission.

In the present study we used computational modelling to study the transmission from the basal ganglia to the thalamus via postinhibitory rebound spikes. We found that uncorrelated basal ganglia output ensures a clear transmission of motor commands with low trial-to-trial variability in the thalamic response latency. In contrast, pathological correlations in SNr led to a noisy transmission with high trial-to-trial variability. In addition, we found that sensory responses in SNr can, depending on their timing relative to the movement-related decrease, either facilitate or suppress rebound spikes leading to promote or suppress movement. Therefore, in the rebound transmission mode, uncorrelated activity and sensory responses in the basal ganglia output have functional roles in the coordinated transmission of motor signals. Finally, we found that the rebound spiking mode persisted in the presence of excitation that is strong enough to maintain baseline firing rates reported in vivo (Bosch-Bouju et al., 2014).

Materials and Methods

Model neuron

In this study we used a Hodgkin-Huxley type model of a thalamocortical neuron (Rubin and Terman, 2004). The model has four different ionic currents: a leak current (I_L), a Na^+ current (I_{Na}), a K^+ current (I_K), and a T-type Ca^{2+} current (I_T), which are determined by the membrane potential v, the channel conductances g and reversal potentials E). While the conductance of the leak current g_L is constant, the conductance of the Na^+, K^+ and T-type Ca^{2+} currents depends on the membrane potential and varies over time. These voltage-dependent conductances are formed by the product of the maximum channel conductance (g_{Na}, g_K and g_{Ca}) and the voltage-dependent (in)activation variables (m, h, p and r).

The model neuron's membrane potential is described by

$$C_m \frac{dv}{dt} + I_L + I_{Na} + I_K + I_T + I_{SNr \to TC} + I_{CX \to TC} = 0 \quad (1)$$

with a leak current $I_L = g_L[v - E_L]$. The Na^+ current $I_{Na} = g_{Na} m_\infty^3(v) h[v - E_{Na}]$ has an instantaneous activation gating variable $m_\infty(v) = \frac{1}{1+\exp(-(v+37)/7)}$ and a slow inactivation gating variable h with $\frac{dh}{dt} = \frac{h_\infty(v)-h}{\tau_h(v)}$ and steady-state $h_\infty(v) = \frac{1}{1+\exp((v+41/4))}$ that is approached with a time constant $\tau_h(v) = \frac{1}{a_h(v)+b_h(v)}$; $a_h(v) = 0.128\exp(-(v+46)/18)$, $b_h(v) = \frac{4}{1+\exp(-(v+84)/4)}$.

The activation variable of the K^+ current $I_K = g_K[0.75(1-h)^4][v - E_K]$ is described in analogy to the Na^+ inactivation variable (h), which reduces the dimensionality of the model by one differential equation (Rinzel, 1985a).

The T-type Ca^{2+} current $I_T = g_T p_\infty^2(v) r[v - E_T]$ has an instantaneous activation $p_\infty(v) = \frac{1}{1+\exp(-(v+60)/6.2)}$ and slow inactivation $\frac{dr}{dt} = \frac{r_\infty(v)-r}{\tau_r(v)}$ with the steady-state $r_\infty(v) = \frac{1}{1+\exp((v+84)/4)}$ and time constant

$$\tau_r(v) = 28 + 0.3(-(v+25)/10.5).$$

The T-type Ca^{2+} channel can cause post-inhibitory rebound spikes by the following mechanism. Prolonged hyperpolarisation leads to de-inactivation of the T-type Ca^{2+} channel, i.e. the inactivation gate (r) opens while the activation gate (p) closes. After shutting down the hyperpolarisation, the inactivation gate closes slowly whereas the activation gate opens very fast. Therefore, while both gates are open, the T-type Ca^{2+} channel briefly opens, leading to a membrane depolarisation. If this depolarisation is strong enough, this can lead to Na^{+} spikes, which are then referred to as post-inhibitory rebound spikes.

The thalamic model neuron receives two types of synaptic inputs; one inhibitory from the basal ganglia output region SNr ($SNr \rightarrow TC$) and one excitatory from cortex ($CX \rightarrow TC$). Synaptic currents I_X are described by a simple exponential decay with the decay rate β_X, where X denotes the synapse type (Gerstner and Kistler, 2002). Similar to the intrinsic ionic currents, each synaptic current is described in terms of the membrane potential v, channel conductance g_X, and the reversal potential v_X: $I_X = g_X[v - v_X]\sum_j s_j$; $X = \{SNr \rightarrow TC, CX \rightarrow TC\}$. When a presynaptic neuron j spikes at time t_i, s_j becomes 1 and decays with time constant β afterwards $\frac{ds_j}{dt} = (1 - s_j)\delta(t - t_i) - \beta_X s_j$, where $\delta(t)$ is the Dirac delta function. With the conductance caused by a single presynaptic spike ($s_j = 1$) given by g_X, the net synaptic current is therefore the sum of all presynaptic events s_j multiplied by g_X and the difference between the membrane potential and synaptic reversal potential. In our model, the reversal potential for the inhibitory synapse is $v_{SNr \rightarrow TC} = -85mV$ (Rubin and Terman, 2004), which is required by the model to generate rebound spikes. This reversal potential,

116 though very hyperpolarised, is in the range of the reversal potentials of thalamocortical neurons in
117 the thalamus (Huguenard and Prince, 1994; Ulrich and Huguenard, 1997; Herd et al., 2013) and is
118 in line with the presence of thalamic rebound spikes in vivo (Kim et al., 2017). The intrinsic and
119 synaptic parameters of the model neuron are described in Table 1.

Table 1. Model parameters

Parameter type	Parameter, value and unit
Ionic channel conductance	$g_L = 0.05\ nS/\mu m^2$ $g_{Na} = 3\ nS/\mu m^2$ $g_T = 5\ nS/\mu m^2$ $g_K = 5\ nS/\mu m^2$
Ionic channel reversal potential	$E_L = -70\ mV$ $E_{Na} = 50\ mV$ $E_T = 0\ mV$ $E_K = -90\ mV$
Synaptic reversal potential	$v_{SNr\to TC} = -85\ mV$ $v_{CX\to TC} = 0\ mV$
Synaptic decay constant	$\beta_{SNr\to TC} = 0.08\ ms^{-1}$ $\beta_{CX\to TC} = 0.18\ ms^{-1}$

Parameters were taken from Rubin and Terman, 2004 and Ermentrout and Terman, 2010.

120 *Input spike trains*

We generated uncorrelated and correlated Poisson spike trains as inputs to the model neuron. To generate uncorrelated spike trains we simulated N independent Poisson processes, each with a firing rate r. We generated the correlated input spike trains for a given average pairwise correlation among them, denoted by ε. However, for $N \geq 3$ different realisations of spike trains with different correlations of order 3 or higher are possible (Kuhn et al., 2003). For a convenient parametrisation of the order of correlation, we used the distribution of the number of coincident spikes, referred to as spike amplitudes (A), in a model of interacting Poisson processes (Staude et al., 2010). For a homogeneous population of spike trains, the average pairwise correlation depends on the first two moments of the amplitude distribution f_A:

$$\varepsilon = \frac{\frac{E[A^2]}{E[A]} - 1}{N - 1} \tag{2}$$

In the present study, we considered binomial and exponential amplitude distributions (Figure 1). While the binomial amplitude distribution has a high probability density around the mean of the distribution (Figure 1A), the exponential distribution has a higher probability density toward smaller amplitudes (Bujan et al., 2015, Figure 1B).

To generate spike trains with a binomial amplitude distribution we implemented a multiple interaction process (Kuhn et al., 2003, Figure 1A). For correlated outputs ($\varepsilon > 0$), this was done by first generating a so-called "mother" spike train, a Poisson spike train with rate λ. We then took this mother spike train to derive the set of spike trains used in our simulations as convergent

inputs to the model neuron. Each spike train in this set was derived by randomly and independently copying spikes of the "mother" spike train with probability ε. The firing rate of each spike train generated via this algorithm is $r = \varepsilon\lambda$.

We also generated spike trains using exponentially distributed amplitudes described by:

$$f_A(\xi;\tau) = \frac{e^{-\tau\xi}}{\sum_{k=1}^{N} e^{-\tau k}}; \xi \in [1,\ N] \tag{3}$$

where $f_A(\xi;\tau)$ is the amplitude distribution with the parameter τ. According to Eq. 2, to compute ε for this distribution, we needed to compute the proportion of the second moment to the first moment for this distribution. We used $E[A^n] = \sum_{\xi=1}^{N} \xi^n f_A(\xi)$ to compute the first and second moments of the distribution and then applied it into Eq. 2, rewriting it to

$$\varepsilon = \frac{\frac{\sum_{\xi=1}^{N} \xi^2 e^{-\tau\xi}}{\sum_{\xi=1}^{N} \xi e^{-\tau\xi}} - 1}{N-1} \tag{4}$$

This equation shows that ε depends on τ and we took a simple numerical approach to find τ for each desired ε. We computed ε for a range of τ (from 0 to 5 with steps of 0.001) and then selected the τ that yielded an ε closest to our desired ε (Figure 1C). The maximum error between the ε we calculated using Eq. 4 and the desired ε was 5×10^{-4}.

The next step was to generate the population spike trains using the probability distribution determined by the τ we already computed. We drew N independent Poisson spike trains each

with rate $r_\xi = Nrf_A(\xi)/\xi;\ \xi \in [1,\ N]$. Since ξ represents the number of coincident spikes in a time bin, spike times from independent spike trains should be copied ξ times to get the final population spike train used as inputs to the model neuron. As the amplitude distribution described in Eq. 3 has a high probability density toward lower amplitudes, high average pairwise correlations cannot be achieved. For typical parameters of the inhibitory input spike trains in this study ($N = 30$, $r = 50$ Hz), the maximum average pairwise correlation was less than 0.65 (Figure 1C).

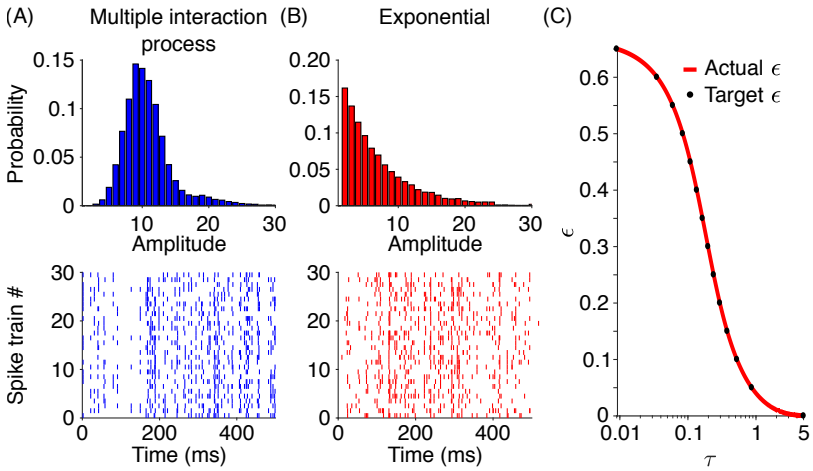

Figure 1. Generation of correlated Poisson spike trains used as input to the model neuron. (A, top) The amplitude distribution of the higher-order correlations was determined for spike trains generated by a multiple interaction process with $\varepsilon = 0.3$ and $r = 50$ Hz. The bottom panel shows the raster plot of 30 respective example spike trains. (B, top) Alternatively, the amplitude distribution of higher-order correlations followed an exponential amplitude distribution with $\varepsilon = 0.3$ and $r = 50$ Hz, and corresponding example spike trains (bottom panel). (C) The parameter τ of the exponential amplitude distributions determined the resulting average pairwise correlation ε (red trace). Black dots represent the average pairwise correlations that we used to generate input spike trains with an exponential amplitude distribution.

158 *Input spike trains with mixture of binomial and exponential amplitude distributions*

159 We computed the spike amplitude distribution of SNr model neurons using a large-scale network
160 model of the basal ganglia (Figure 2D; see also below). This amplitude distribution involved a
161 mixture of exponential and binomial distributions leading to an average pairwise correlation of
162 0.6 (black dot in Figure 2). To obtain spike trains following this mixed distribution, we first
163 created one spike train with an exponential amplitude distribution contributing 20% of the spikes
164 with an average pairwise correlation of 0.25. Next, another spike train with a binomial amplitude
165 distribution was generated (see above), contributing the remaining 80% of the spikes in the input
166 spike train. We changed the average pairwise correlations of these input spike trains by only
167 changing the average pairwise correlation of the subset with the binomial amplitude distribution.

168 *Uncorrelated input spike trains with gradual decrease*

169 We captured the gradual movement-related decrease, which is observed experimentally, by using
170 a sigmoid function to describe the firing rate of the input spike trains as a function of time $r(t) =$
171 $50(1 - 1/[1 + e^{-a(t-t_{mov})}])$ Hz. We varied the slope parameter, a, to change the slope of the firing
172 rate decrease. t_{mov} is the time point (in this study at one second), when the firing rate decreases to
173 the half maximum, i.e. $r(t_{mov}) = 25$ Hz.

174 *Data analysis: identifying rebound spikes*

175 The model neuron can fire spikes in response to excitatory input or due to release from inhibition

with post-inhibitory rebound spikes. Therefore, one challenge was to distinguish "normal" spikes driven by excitatory inputs from post-inhibitory rebound spikes. In mice studies, genetic approaches are often used to knockout T-type Ca^{2+} channels, which are critical for generation of post-inhibitory rebound spikes (Kim et al., 2017). We adopted this in our model by simply removing the T-type Ca^{2+} channels in our model (i.e. $g_T = 0\ nS/\mu m^2$). However, this also caused changes in the intrinsic properties of the model neuron such as its excitability. We therefore took a more elaborate approach tailored to each of the two excitation scenarios, single excitatory spikes (Figure 5) and spontaneous excitation (Figure 6).

For the simulations with a single excitatory input spike the identification of rebound spikes was straightforward because the used excitatory strengths were subthreshold and thus could evoke no spikes. Therefore, we labelled all generated spikes as rebound spikes. However, for the simulations with ongoing excitation, the excitatory input was able to evoke "normal" spikes as well. To identify rebound spikes there, we simulated the model neuron with three different input combinations, inhibition-only, excitation-only and inhibition-excitation. For inhibition-only input, we determined the output firing rate of the model neuron purely due to rebound spiking (f_I). In addition, we determined the time window in which the model neuron fired those rebound spikes (as this was typically in a short time window just after the movement-related decrease). We then compared the rebound-driven firing rate in this time window with the firing rate f_E obtained from an excitation-only simulation (i.e. without any inhibitory input, so no rebound spikes). Finally, we fed our model with both inputs (inhibition-excitation) and computed the firing rate in that time window,

196 which involved both rebound and non-rebound spiking (f_{EI}). We then computed the proportion of
197 rebound spiking as: $\frac{f_{EI}-f_E}{f_I}$.

198 *Data analysis: transmission quality*

199 For our simulations shown in Figure 2, we needed to quantify the transmission quality for a variety
200 of inputs strengths and degrees of correlation. For a clear transmission of the motor signal the
201 thalamocortical neuron would ideally respond only to the movement-related decrease of activity
202 in SNr neurons with a rebound spike, and be silent otherwise. Any rebound spike before the
203 movement-related decrease would make the transmission noisy, in the sense that the decoding of
204 the presence and timing of the motor signal in thalamic activity would be less accurate. Therefore,
205 we used the number of spikes after the onset of the movement-related decrease, normalised by the
206 total number of spikes within -1 s to 0.5 s around the onset of the movement-related decrease as a
207 measure of the transmission quality.

208 *Large-scale model of the basal ganglia*

209 We utilised a large-scale network model of the basal ganglia (Lindahl and Kotaleski, 2016) to
210 compute the distribution of spike amplitudes in SNr during pathological activity in dopamine-depleted
211 basal ganglia. This network model mimics the pathological activity pattern observed experimentally
212 in a rat model of Parkinson's disease. To achieve the pathological activity pattern in SNr, we ran
213 this model using a default parameter set originally from this network model. This parameter set
214 involved setting dopamine modulation factor to zero and inducing a 20-Hz modulation to the

emulated cortical inputs to the basal ganglia regions (for details see Lindahl and Kotaleski, 2016).

Software packages

We implemented the model neuron in Simulink, a simulation package in MATLAB (R2016b) and used a 4th-order Runge-Kutta method to numerically solve the differential equations (time step = 0.01 ms). We wrote all scripts to generate input spike trains, handle simulations and analyse and visualise the simulation data in MATLAB. To run the simulations we used the "NEMO" high-performance computing cluster in the state of Baden-Wuerttemberg (bwHPC) in Germany.

Code accessibility

We provided our simulation scripts (in "BasicModelSimulations" directory) including the scripts generating input spike trains (in "SpikeTrains" directory) accessible via a git repository `https://github.com/mmohaghegh/NigrothalamicTransmission.git`

Results

Uncorrelated activity promotes the transmission of motor signals

To determine whether uncorrelated activity in basal ganglia output is important for the transmission of motor signals, we simulated a thalamocortical neuron exposed to inhibitory Poisson input spike trains with varying degrees of correlation (Figure 2). We used binomial and exponential amplitude distributions to generate correlated Poisson spike trains (see Materials and Methods). In addition,

we modulated the input firing rate so that it mimicked the prominent movement-related decrease of basal ganglia output neurons observed in experimental studies (Hikosaka and Wurtz, 1983; Schultz, 1986; Leblois et al., 2007; Schmidt et al., 2013).

For uncorrelated inputs the model responded to the movement-related decrease with a single rebound spike (Figure 2A, left panel). However, for correlated inputs rebound spikes appeared not only after the movement-related decrease, but also at random times during baseline activity (Figure 2A, middle and right panels). The reason for this was that correlated SNr activity led not only to epochs with many synchronous spikes, but also to pauses in the population activity that were long enough to trigger rebound spikes.

In mammals multiple inhibitory projections from SNr converge on a single thalamocortical neuron (Edgerton and Jaeger, 2014), which affects the strength of the inhibition on the thalamocortical neuron. Since the degree of convergence is not known, we repeated our simulations for different inhibitory strengths, but found that the transmission quality did not depend on the inhibitory strength as long as the inhibition was strong enough to lead to rebound spikes (Figure 2D). Furthermore, as for more than two inputs the input spike trains cannot be uniquely characterised by pairwise correlations, we considered two different possibilities for higher-order correlations (see Materials and Methods). We found that the transmission quality strongly depended on both the input average pairwise correlation and higher-order correlations among input spike trains (Figure 2B).

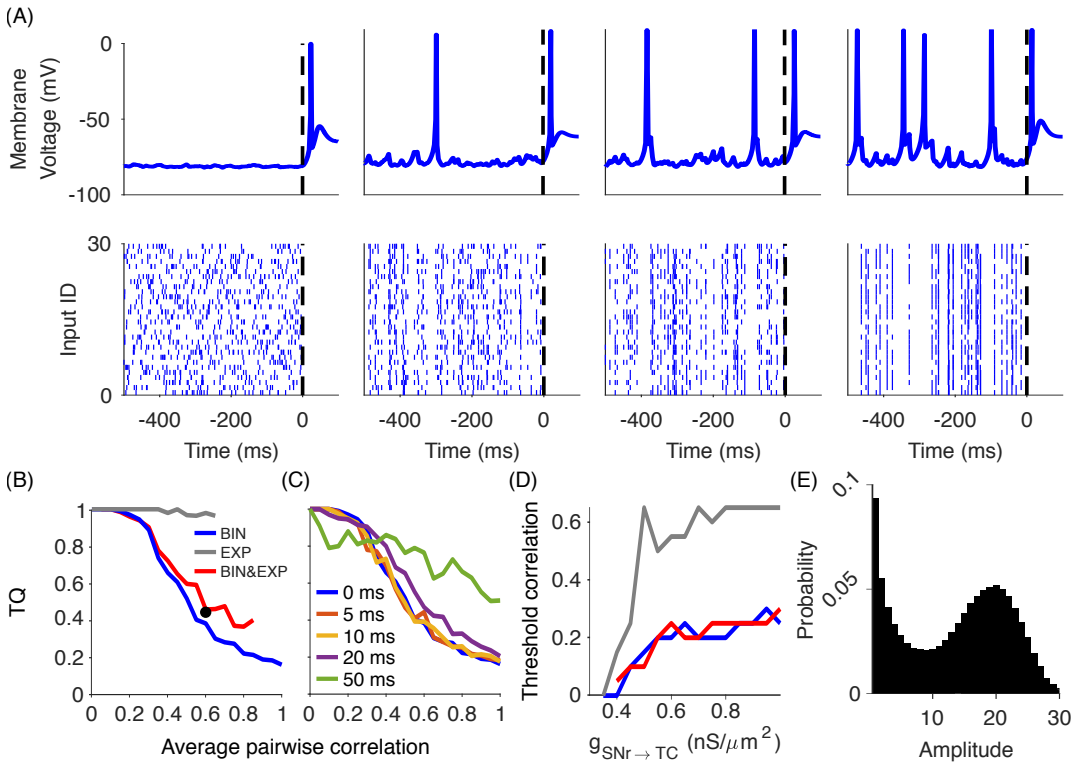

Figure 2. Input spike correlations impair the transmission quality (TQ) of motor signals from SNr to thalamus. (A) Top panels show the intracellular response of the thalamocortical model neuron to the inhibitory input spike trains from SNr displayed in the bottom panels. Uncorrelated Poisson spike trains ($\varepsilon = 0$) led to clear transmission (TQ = 1) via a single rebound spike after the firing rate decrease in the input (leftmost panel). Correlated Poisson spike trains, however, led to rebound spikes at random times, whenever there is a pause in the input spike trains (left middle panel: $\varepsilon = 0.2$ leading to TQ = 0.5, right middle panel: $\varepsilon = 0.35$ leading to TQ = 0.33 and rightmost panel: $\varepsilon = 0.7$ leading to TQ = 0.25). (B) Impact of input correlations on TQ depended on the correlation model (BIN, binomial; EXP, exponential; BIN&EXP, mixture of both). Note that the exponential amplitude distribution had a maximum average pairwise correlation of 0.65 (see Materials and Methods). The black dot marks the TQ for the spike trains generated using the amplitude distribution shown in (E). (C) For the binomial correlation model, jittering the input spike times decreased the TQ only for long jitter time windows (50ms), indicating that correlations on longer time scales are overall less detrimental. (D) The threshold correlation at which the transmission quality deteriorated (TQ$<$ 0.95) only weakly depended on the inhibitory input strength (same legend as in B). (E) The simulation of Parkinson's disease in a large-scale model of the basal ganglia yielded an amplitude distribution of SNr spike times that corresponded to a mixture of the exponential and binomial amplitude distributions.

Pairwise correlations affected the transmission for a binomial amplitude distribution (Figure 2B, dark blue trace). For a binomial amplitude distribution higher-order events ("population bursts") are common, which increases the probability for pauses in the population activity. Thereby, even weak correlations among SNr spike trains led to a sharp decrease in the transmission quality. In contrast, for spike train correlations with an exponential amplitude distribution, the decrease in transmission quality was less pronounced (Figure 2B, grey trace). This was because for the exponential amplitude distribution lower-order events are more common, which are not sufficient for pauses in the population activity of SNr neurons leading to thalamic rebound spikes. Therefore, in particular higher-order correlations may be detrimental for the transmission of motor commands.

We further investigated whether the substantial decrease in the transmission quality observed for the binomial amplitude distribution depended on millisecond synchrony of correlated spike times. We jittered the synchronous spike events using different time windows (Figure 2C), which corresponds to correlations on slower timescales. We found that the transmission quality decreased for jittering timescales $\leq$ 20 ms similar to inputs with correlations on a millisecond timescale (i.e. without jittering), confirming that the decrease in transmission quality does not depend on millisecond synchrony. However, correlations on the timescale of 50 ms did not substantially influence the transmission quality, as was expected due to the lack of population pauses.

The purpose of our simulation of correlated activity was to mimic basal ganglia output patterns in Parkinson's disease. However, as the amplitude distribution of pathologically correlated activity in SNr is currently unknown, we employed a large-scale model of the basal ganglia (Lindahl and

Kotaleski, 2016), in which beta oscillations propagate through cortico-basal ganglia circuits (see Materials and Methods). Beta oscillations are widely observed in animals with dopamine-depleted basal ganglia including their output nuclei (Brown et al., 2001; Avila et al., 2010). While beta oscillations can be generated in the pallido-subthalamic loop (Mirzaei et al., 2017), here we did not assume a specific mechanism for the generation of correlated activity in Parkinson's disease, but focussed on the amplitude distribution in SNr in a simulation of Parkinson's disease. We found that the amplitude distributions in the dopamine-depleted state of the large-scale model were somewhere in between binomial and exponential (Figure 2E).

To investigate the model with a correlation structure that might be relevant for Parkinson's disease, we generated input spike trains based on a mixture of binomial and exponential distributions (see Materials and Methods). We then investigated the effect of different average pairwise correlations in this mixed distribution. We found that increasing the average pairwise correlation of the binomial component of the mixed distribution had a similar effect on the transmission quality as in the standard binomial amplitude distribution (Figure 2B, red and blue traces). Furthermore, for the average pairwise correlation found from the large-scale model for Parkinson's disease the transmission quality was low (Figure 2B, black dot). This confirms that under a correlation structure similar to Parkinson's disease, even weak correlations in basal ganglia output can impair the transmission of motor signals, potentially related to motor symptoms such as tremor or akinesia (Magnin et al., 2000; Edgerton and Jaeger, 2014; Kim et al., 2017).

Uncorrelated activity increases transmission speed

To study the effect of input correlations on transmission speed, we used the same scenario as above (Figure 2) and measured the time between the onset of the movement-related decrease and the rebound spike. We found that the transmission speed was fastest for no or weak correlations, and slower for stronger correlations (Figure 3A). Therefore, uncorrelated activity in basal ganglia output regions may also promote the fast transmission of motor signals. To generalise our findings on the transmission speed beyond the scenario using the movement-related decrease, we further examined transmission speed using (rebound) spike-triggered averages of inputs. Instead of simulating a movement-related decrease, we exposed the model neuron to inhibitory inputs with a constant firing rate. To compute the spike-triggered average, we used the peak of each rebound spike as the reference time point to compute the average of the preceding input. Since rebound spikes occurred more often for stronger input correlations, we performed this analysis on inputs having a correlation coefficient of either 0.3 or 1.0. These simulations confirmed that weak input correlations induce faster transmission than strong correlations (Figure 3C).

Uncorrelated activity decreases transmission variability

For the transmission of motor signals via rebound spikes the trial-to-trial variability of the transmission speed may be important. For example, to coordinate motor signals across different neural pathways low variability (i.e. high precision) of the transmission speed might be necessary. To investigate the nigrothalamic transmission variability, we computed the variance over the latencies across 100 trials with movement-related decreases in SNr activity (i.e. the same scenario as in Figure 3A). We found that for uncorrelated inputs transmission was very precise in the

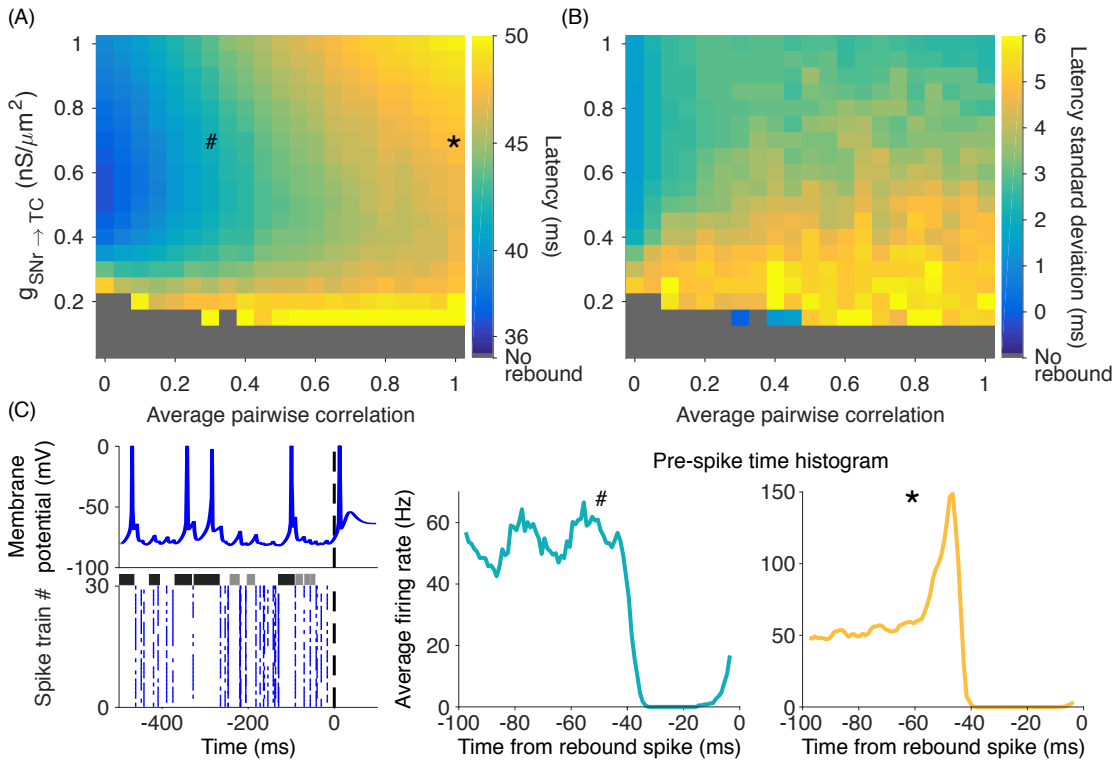

Figure 3. Correlated SNr spike trains decrease transmission speed and temporal precision of rebound spikes. Systematic investigation of average transmission latency (A) and its standard deviation (B) for different degrees of correlation and inhibitory strengths identified the range with fastest transmission speed and highest transmission precision, respectively. (C) Left panel shows a sample membrane potential ($g_{SNr\rightarrow TC} = 0.70\ nS/\mu m^2$, $\varepsilon = 0.7$; top) of the thalamocortical model neuron and the corresponding inhibitory inputs (bottom). Note that rebound spikes were preceded by pauses in the input raster plot (indicated by black horizontal bars). However, for very short pauses (indicated by grey horizontal bars) no rebound spikes occurred. Averages triggered by rebound spikes for weakly correlated inputs (C, middle panel) and strongly correlated inputs (C, right panel) confirmed that pauses in the inhibitory input preceded rebound spikes. The duration of the pause preceding the rebound spikes reflected the transmission latency. The inset symbols (#, *) in (A) indicate the parameters used for the corresponding spike-triggered averages in (C).

sense that the trial-to-trial variability of the response latency was small (Figure 3B). In contrast, even weak correlations led to a high transmission variability due to changes in the amount of hyperpolarisation caused by correlated inputs preceding rebound spikes. We conclude that uncorrelated inputs ensure a high precision of the transmission via rebound spikes by reducing the trial-to-trial variability in response latency.

Sensory responses can promote or suppress rebound spiking

SNr neurons often have short-latency responses to salient sensory stimuli characterised by brief increases in firing rate (Pan et al., 2013). In rats performing a stop-signal task these responses also occurred in neurons that decreased their activity during movement (Schmidt et al., 2013). This included responses to auditory stimuli, which cued the initiation of a movement (Go cue) or the cancellation of an upcoming movement (Stop cue). We examined how such brief increases in SNr activity affect rebound spiking in the thalamocortical model neuron (Figure 4). The thalamocortical model neuron received inputs similar to the SNr firing patterns recorded in rats during movement initiation (i.e. uncorrelated inputs with high baseline firing rate and a sudden movement-related decrease). To model sensory responses in the SNr neurons, we added a brief increase in firing rate at different time points relative to the movement-related decrease (Figure 4A). We generated the brief increase by adding a single spike in each spike train having the sensory response at the desired time point. This allowed us to observe the effect of the timing of sensory responses on rebound spiking.

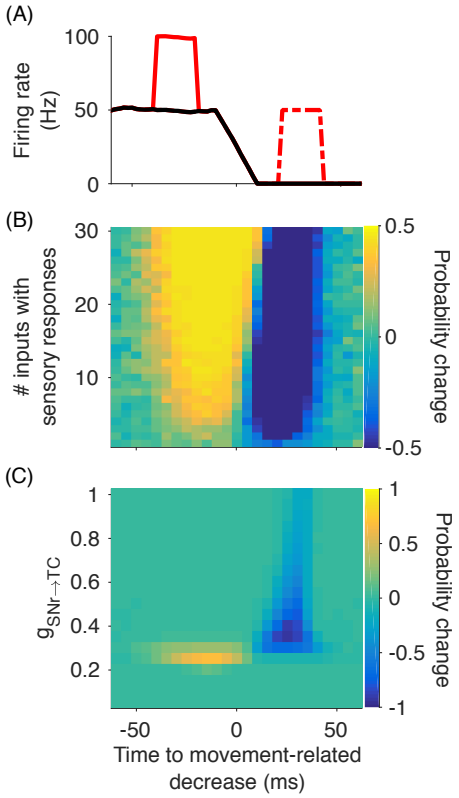

Figure 4. Sensory responses in SNr firing rate change the probability of rebound spikes in the thalamocortical model neuron. (A) The simulations used an average firing rate as input, which reflected the SNr firing rate with a movement-related decrease (black line). Sensory responses (red lines) were then added to the input at different time points relative to the movement-related decrease. Here two example timings are shown, before (solid) and after (dash-dot) the movement-related decrease. (B) The timing of the sensory responses relative to the movement-related decrease was varied systematically (x-axis). For a given relative timing, we determined whether rebound spikes were suppressed (blue area) or facilitated (yellow area; here $g_{SNr\rightarrow TC} = 0.29\ nS/\mu m^2$). Note the large impact of the timing of the sensory response on the probability of rebound spikes, even if it occurred in only a small subset of neurons. (C) The input strength $g_{SNr\rightarrow TC}$ affects the suppression and facilitation of rebound spikes. Here the change in rebound probability was averaged across the number of inputs with sensory responses (across y-axis in B).

To quantify the effect of sensory responses, we measured the difference in the probability of generating a rebound spike after the movement-related decrease in simulations with and without sensory responses. Interestingly, the sensory responses could either increase or decrease the probability of generating a rebound spike, depending on their relative timing to the movement-related decrease (Figure 4B). For sensory responses preceding the movement-related decrease for up to 40 ms, the probability of generating a rebound spike was increased. This was because the sensory response led to additional hyperpolarisation in the thalamocortical neuron, which promoted rebound spiking. In contrast, for sensory responses occurring 10-40 ms after the movement-related decrease, the probability of generating a rebound spike was decreased. This was because the sensory response in that case partly prevented the movement-related pause of SNr firing. Together, this points to the intriguing possibility that sensory responses in SNr can have opposite effects on behaviour (either promoting or suppressing movement), depending on their timing (Figure 4B). This could explain why SNr neurons respond to both Go and Stop cues with a similar increase in firing rate (Schmidt et al., 2013; Mallet et al., 2016), a previously puzzling finding (see Discussion).

In addition to the timing of sensory responses relative to the movement-related decrease, also the inhibitory input strength modulated the probability of generating a rebound spike (Figure 4C). For weaker inhibitory inputs ($g_{SNr\rightarrow TC} = 0.25nS/\mu m^2$), the probability of generating a rebound spike was increased because the additional inhibitory inputs contributed to the hyperpolarisation of the thalamocortical neuron. However, for slightly stronger inputs ($g_{SNr\rightarrow TC} \geq 0.35nS/\mu m^2$), the sensory responses could not further facilitate rebound spiking because the probability of generating

a rebound spike was already one. Accordingly, sensory responses were most effective in reducing the probability of generating a rebound spike for medium input strengths (i.e. with a relatively high probability of generating a rebound spike). We found that the most effective strength for suppressing rebound spikes was at $g_{SNr\to TC} = 0.35nS/\mu m^2$. However, the suppressing effect vanished for $g_{SNr\to TC} \geq 0.8nS/\mu m^2$ because for this strength the sensory responses themselves caused a hyperpolarization strong enough to trigger a rebound spike (Figure 4C). Therefore, the effect of sensory responses in SNr on motor signals strongly depended on the nigrothalamic connection strength.

Rebound spikes in the presence of excitation

Having studied basic properties of rebound spiking in the model under somewhat idealised conditions, we next extended the model to account for further conditions relevant in vivo. For example, we have assumed so far that the thalamocortical neuron receives input from SNr neurons that decrease their activity during movement. However, electrophysiological recordings in SNr and other basal ganglia output neurons have also identified neurons that do not decrease their activity during movement (Schmidt et al., 2013). Therefore, we investigated the response of the thalamocortical model neuron in a scenario in which only a fraction of SNr inputs decreased their firing rates, while the remaining neurons did not change their rates (Figure 5). We found that the thalamocortical model neuron elicited a rebound spike with high probability only when a large fraction of input neurons decreased their firing rates to zero (Figure 5A).

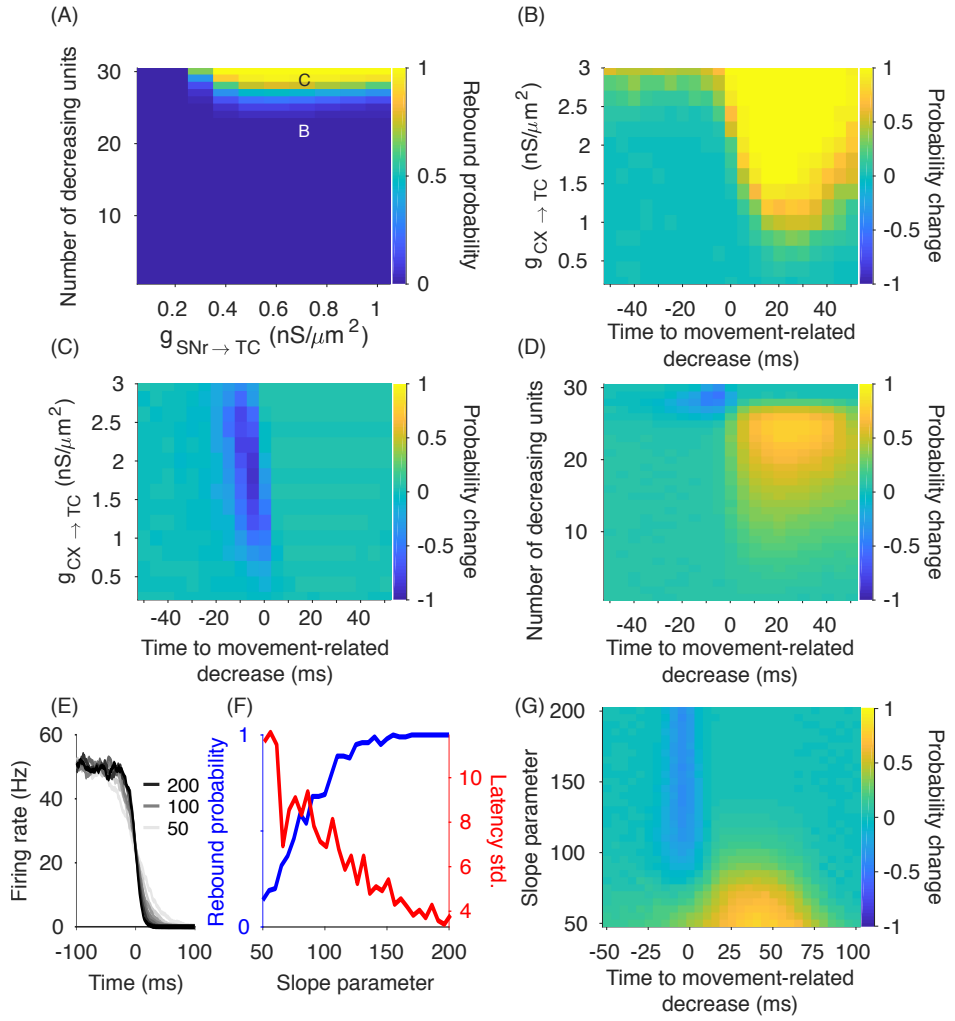

Figure 5. Effect of excitatory input spike timing on rebound spiking. (A) Rebound spikes occurred only when a large fraction of inhibitory input spike trains exhibited a movement-related decrease in firing rate, even for strong inhibitory inputs. (B) Single excitatory input spikes increased the probability of rebound spikes compared to pure inhibitory inputs (letter "B" in panel A) when they were presented briefly after the movement-related decrease (x-axis). Note that this occurred in a regime, in which usually no rebound spike were generated because not enough neurons decreased their firing rate (here 22 out of 30). (C) In contrast, in a regime in which rebound spikes were often generated (letter "C" in panel A), adding a single excitatory spike as input to the thalamocortical neuron decreased the probability of rebound spikes compared to pure inhibitory inputs, when they were presented briefly before the movement-related decrease (x-axis). (D) Systematic investigation of the parameter space indicated a narrow regime, in which single excitatory spikes can decrease, and a larger regime, in which they can increase the probability of a rebound spike. The change in probability was averaged over excitatory input strengths (i.e. over the y-axis in B and C). (E) SNr firing rate decreases with different slopes were generated by varying the indicated slope parameter *a* (see Methods). (F) Smaller SNr firing rate slopes reduced the probability of rebound spikes and increased the standard deviation of the rebound spike latencies across trials. (G) Single excitatory input spikes typically decreased the probability of rebound spikes for steep movement-related decreases in firing rate (i.e. high slopes), and increased the probability of rebound spikes for more gradual decreases.

The large fraction of SNr neurons required to exhibit a movement-related decrease in order to elicit a rebound spike downstream constrains the scenario under which this transmission is plausible in vivo. However, in a more realistic scenario the thalamocortical neuron also receives excitatory inputs (e.g. from cortex). Therefore, we examined whether excitatory input can, under some conditions, enhance the transmission via rebound spiking (Figure 5B-D). Importantly, the excitatory inputs should be weak enough in order not to elicit spikes themselves. We simulated the model neuron by adding a single excitatory input spike with variable timing with respect to the movement-related decrease in the inhibitory inputs, and observed whether it promoted or suppressed rebound spikes. We investigated the effect of the excitatory spike on the probability of generating a rebound spike by comparing a simulation including excitatory and inhibitory inputs with a simulation that included only inhibitory inputs. We found that for parameter regions in which the probability of generating a rebound spike was usually small (i.e. in the dark blue region in Figure 5A), additional excitatory spikes after the movement-related decrease increased the rebound probability (Figure 5B). We confirmed that these spikes in the thalamocortical neuron are actually rebound spikes (and not just driven by the excitatory input; see Materials and Methods). However, for strong excitation, the thalamocortical model neuron spiked also before the SNr movement-related decrease, indicating that these spikes were no longer rebound spikes.

For parameter regions in which the probability of generating a rebound spike was high (i.e. outside the dark blue region in Figure 5A), the excitatory input spikes could also suppress the generation of rebound spikes when they occurred before the movement-related decrease (Figure 5C). In contrast,

when the excitatory input spike occurred after the movement-related decrease, it enhanced the probability of generating a rebound spike. Therefore, similar to the complex effect of sensory responses in SNr neurons described above, also the excitatory input to the thalamocortical neurons could either promote or prevent rebound spikes depending on its timing. Furthermore, if only a fraction of SNr neurons exhibited a movement-related decrease, precisely timed excitatory input could promote the transmission of the motor command to the thalamocortical neuron (Figure 5D). Overall, our simulations indicate that rebound spikes can occur in a broad parameter regime that also includes excitation. Furthermore, precisely timed excitation provides an additional rich repertoire of rebound spike modulation, either promoting or suppressing movement-related rebound spikes.

Role of the slope of the movement-related decrease

So far we assumed that the movement-related decreases in SNr firing rate are abrupt. However, electrophysiological recordings in rodents (Schmidt et al., 2013) and non-human primates (Hikosaka and Wurtz, 1983; Schultz, 1986; Leblois et al., 2007) indicate that, at least in data averaged over trials, the firing rate decreases can also be more gradual. Therefore, we investigated the impact of input spike trains with various slopes (see Methods) on rebound spikes (Figure 5E). We found that steep slopes of the movement-related firing rate decrease led to rebound spikes with high probability and small timing variability (Figure 5F). In contrast, more gradual movement-related decreases reduced the probability of rebound spikes and increased the spike timing variability.

We further investigated the impact of single excitatory spikes (similar to above) on the probability of rebound spikes for different SNr firing rate slopes (Figure 5G). We found that, if the slope was too small to reliably evoke rebound spikes (low rebound probability), excitatory spikes briefly after the onset of the movement-related decrease could increase the probability of rebound spikes. In contrast, for steeper slopes, the probability of rebound spikes decreased when the excitatory spike occurred before the movement-related decrease. These results further support that excitation can powerfully modulate rebound spiking and promote rebound spikes even under circumstances in which the inhibitory input characteristics are by themselves insufficient for the generation of rebound spikes.

Transmission modes revisited: prevalence of rebound spiking

The interaction of excitation and inhibition in thalamocortical neurons is important because even weak excitation may change the transmission mode from rebound to disinhibition (Goldberg et al., 2013). As we observed rebound spiking in the presence of single excitatory spikes (Figure 5), we further investigated how ongoing excitation affects the mode of nigrothalamic transmission. As before, we simulated the model neuron with movement-related inhibitory inputs, but added a background excitation in the form of a Poisson spike train with the firing rate of 100 Hz and examined the effect of changing excitatory strength (Figure 6). In an idealised scenario the model neuron spikes exclusively after the SNr movement-related decrease for both the rebound and disinhibition transmission modes. These spikes are either post-inhibitory rebound spikes (in the rebound mode), or the result of depolarisation through excitation (in the disinhibition mode).

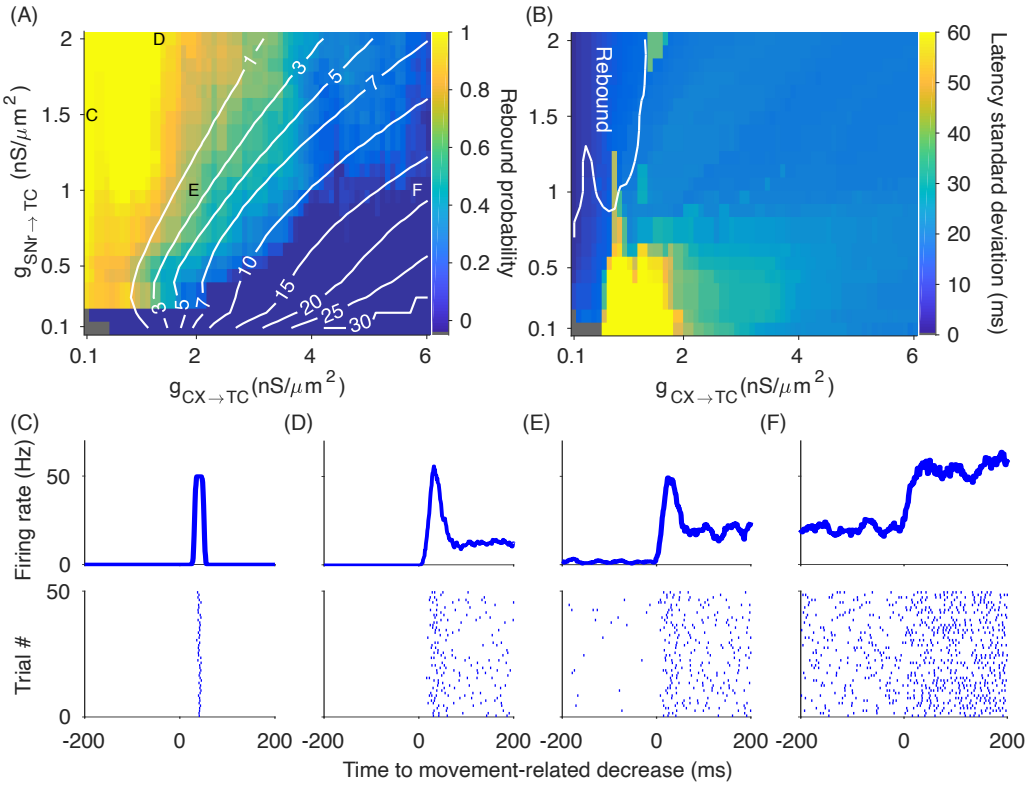

Figure 6. Smooth transition from rebound to disinhibition transmission mode. (A) The probability of rebound spikes only gradually decreased with stronger excitatory inputs, indicating a large parameter regime in which the rebound and disinhibition transmission modes coexisted. The yellow area marks the regime in which transmission was exclusively mediated by rebound spiking, while in dark blue areas the basal ganglia output only disinhibited cortical excitation. The white isolines illustrate the baseline firing rate of the model neuron (i.e. the firing rate before the onset of the movement-related decrease in the input). In the small grey region (bottom left) the model neuron did not fire. (B) The standard deviation of the latency (across trials) of the first thalamocortical spike relative the movement-related decrease distinguished rebound from disinhibition transmission modes. For the rebound mode (i.e. yellow area in A) the standard deviation was almost always the lowest, and the regime in which rebound and disinhibition coexisted the standard deviation was markedly higher. White contour line shows the boundaries of the yellow area in panel (A), where the transmission was exclusively mediated by rebound spiking. (C-E) Sample firing rate profiles and corresponding raster plots show the activity of the thalamocortical neuron in different parts of the parameter regime (as indicated by the corresponding letters in A) with rebound spiking only (C), coexistence of rebound and disinhibition (D-E) and disinhibition only (F).

However, we found that rebound and disinhibition modes could also coexist in regimes in which the model neuron has non-zero baseline firing rates (Figure 6A).

We characterised the nigrothalamic transmission mode (see Materials and Methods) according to the proportion of trials with rebound spikes for a range of inhibitory and excitatory inputs strengths (Figure 6A). Motor signals were transmitted via rebound spikes even in the presence of weak excitatory inputs ($g_{CX \rightarrow TC} \leq 1.5\ nS/\mu m^2$; Figure 6A). Interestingly, the transition from rebound to disinhibition mode was not abrupt, but there was a region where disinhibition and rebound spikes coexisted (Figure 6B). In these overlapping regions rebound spiking seemed to be the dominant firing pattern with a strong, transient firing rate increase in response to the movement-related decrease, a phenomenon which was already observed in anesthetised songbirds (Kojima and Doupe, 2009; Figure 6D, E; see also Discussion). We also examined the effects of varying the firing rate of the excitatory inputs (200, 500, and 1000 Hz). While the rebound and disinhibition spiking mode still overlapped, the corresponding parameter region was shifted towards lower excitatory conductances. For moderate excitatory input firing rates (100 and 200 Hz), rebound spiking occurred also in regions in which the model neuron was spontaneously active (Figure 6E). This overlap was present for spontaneous activity up to 3 Hz in line with the average spontaneous firing of motor thalamus neurons in rats during open-field behavior (Bosch-Bouju et al., 2014). However, for higher spontaneous activity (>7 Hz) rebound spiking vanished (Figure 6F). We conclude that the model neuron can transmit motor signals in the rebound mode in the presence of excitatory inputs.

We also characterised the transmission precision for different transmission modes by computing the standard deviation of the timing of the first spike after the movement-related decrease across trials (Figure 6B). For the rebound transmission mode, the transmission precision was maximal (i.e. minimal timing standard deviation), but as the proportion of trials with disinhibition mode increased, the transmission precision decreased. In the weak inhibition and excitation regime, where rebound and disinhibition modes coexisted and the baseline firing rate of the model neuron was low (< 7 Hz), the precision was smallest. This is important because the spiking variability can be characterised in electrophysiological recordings and may thus provide an indication of the transmission mode *in vivo*.

In summary, our computational model points to new functional roles for uncorrelated basal ganglia output in the clear transmission of motor signals. Furthermore, we have characterised how motor signals transmitted via rebound spikes could either be suppressed or promoted through sensory responses indicating that thalamocortical neurons may be a key site for the integration of sensory and motor signals. Finally, we showed that excitatory inputs to the thalamocortical neurons do not necessarily prevent rebound spiking, but may as well support the generation of rebound spikes.

Discussion

We used computational modelling to study the impact of spike train correlations in the basal ganglia output on the transmission of motor signals. Based on previous studies (Hikosaka and Wurtz, 1983; Schultz, 1986; Leblois et al., 2007; Schmidt et al., 2013), we focused our

description on movement-related pauses in SNr that potentially drive rebound spikes in motor thalamus. However, as e.g. also neurons in the superior colliculus can respond with a rebound spike after prolonged hyperpolarisation (Saito and Isa, 1999), our modelling results might apply more generally. Furthermore, while previous studies identified the important role of excitation in determining regimes in which rebound spikes can occur (Goldberg et al., 2013; Edgerton and Jaeger, 2014), our model produced rebound spikes in a wider parameter regime, also in the presence of excitation (Figure 6). In addition, rebound spiking overlapped with the disinhibition transmission mode, indicating that rebound spiking might apply more widely for nigrothalamic communication in line with recent experimental evidence (Kim et al., 2017). In our model, the impaired nigrothalamic transmission of motor signals for correlated inputs also indicates a potential functional role of active decorrelation in basal ganglia output regions (Wilson, 2013).

Functional role of active decorrelation in the basal ganglia

One prominent feature of neural activity in the healthy basal ganglia is the absence of spike correlations (Bar-Gad et al., 2003). This might be due to the autonomous pacemaking activity of neurons in globus pallidus externa/interna (GPe/GPi), subthalamic nucleus (STN) and SNr, as well as other properties of the network such as heterogeneity of firing rates and connectivity that actively counteracts the synchronisation of activity (Wilson, 2013). While uncorrelated basal ganglia activity may maximise information transmission (Wilson, 2015), our simulations demonstrate that it further prevents the occurrence of random pauses in SNr/GPi activity that

could drive thalamic rebound spikes. Thereby, uncorrelated basal ganglia output activity may ensure that rebound spikes in motor thalamus neurons occur only upon appropriate signals such as the movement-related decreases in basal ganglia output firing rate. In contrast, correlated basal ganglia output activity leads to rebound activity in motor thalamus also at baseline SNr activity, i.e. in absence of any motor signal. This decrease in the signal-to-noise ratio of motor signals may cause problems in motor control.

Evidence for the functional relevance of uncorrelated basal ganglia activity originates from the prominent observation that basal ganglia activity becomes correlated e.g. in Parkinson's disease (Bergman et al., 1998; Nevado-Holgado et al., 2014). Therefore, our simulations with correlated basal ganglia output activity capture a key aspect of neural activity in Parkinson's disease. Interestingly, our finding that basal ganglia correlations increase the rate of motor thalamus rebound spikes is in line with recent experimental findings. In dopamine-depleted mice with Parkinson-like motor symptoms, the rate of motor thalamus rebound spikes was also increased compared to healthy controls (Kim et al., 2017). Furthermore, an increased trial-to-trial variability of rebound spikes was found in dopamine-depleted mice, similar to our simulations (Figure 3).

Therefore, our results support a functional role for active decorrelation in the clear transmission of motor signals with low trial-to-trial variability from the basal ganglia to motor thalamus. In contrast, pathological correlations may lead to unreliable and noisy transmission of motor signals with high trial-to-trial variability, potentially contributing to motor symptoms in Parkinson's disease.

Role of rebound spikes for motor output

In our simulations we only examined the activity of a single thalamocortical neuron. However, for motor signals propagating further downstream, the coordination of activity among different thalamocortical neurons might be relevant. Due to the low trial-to-trial variability of the response latency of rebound spikes in the model (Fig. 6B), pauses in population SNr activity would lead to synchronous rebound spikes among thalamocortical neurons. In contrast, excitatory, Poisson inputs from cortex enhanced trial-to-trial variability (Fig. 6B) and thus would not lead to synchronous activity among thalamocortical neurons. Even though downstream regions cannot directly distinguish thalamic rebound spikes from excitation-driven spikes, they might read out synchronous activity that occurs primarily for rebound spikes. Thereby, only coordinated activity in different thalamocortical neurons may lead to movement initiation (Gaidica et al., 2018) or muscle contraction (Kim et al., 2017). This is in line with the experimental finding showing that, despite no significant difference in the peak or average firing rates of single unit recordings from intact and knockout neurons lacking T-type Ca^{2+} in the motor thalamus, multi unit recordings from intact neurons reached a stronger peak firing rate earlier than the knockout neurons (Kim et al., 2017). This early activation of a greater proportion of intact neurons after the termination of the inhibition, which indicates a coordinated activity across neurons, was accompanied by a muscular response whereas no muscular response was observed in the knockout state (Kim et al., 2017). Therefore, rebound activity in an individual motor thalamus neuron may not lead to muscle contraction, but instead synchronous rebound spikes in several motor thalamus neurons may be

527 required.

528 *Impact of sensory responses on the transmission of motor signals*

529 SNr neurons that decrease their activity during movement also respond to salient sensory stimuli
530 such as auditory "Go" stimuli cueing movement (Pan et al., 2013; Schmidt et al., 2013). One
531 proposed functional role for this brief firing rate increase is to prevent impulsive or premature
532 responses during movement preparation in SNr neurons (Schmidt et al., 2013). In addition, in
533 our model we observed that, depending on the precise timing, sensory responses may also promote
534 thalamocortical rebound spikes and movement. This effect was present when the sensory responses
535 preceded the movement-related decrease by up to 40 ms (Figure 4).

536 In rats performing a stop-signal task the same SNr neurons that responded to the "Go" stimulus
537 also responded to an auditory "Stop" signal, which prompted the cancellation of the upcoming
538 movement (Schmidt et al., 2013). These responses were observed in trials, in which the rats
539 correctly cancelled the movement, but not in trials where they failed to cancel the movement.
540 These SNr responses to the "Stop" signal may delay movement initiation, allowing another
541 slower process to completely cancel the planned movement (Mallet et al., 2016). In line with
542 this "pause-then-cancel" model of stopping (Schmidt and Berke, 2017), we observed that the
543 SNr sensory responses can also prevent rebound spikes when they occur close to the time of the
544 motor signal. In our model this suppression effect was present up to 40 ms after the onset of the
545 movement-related decrease in SNr activity (Figure 4). Thereby, our model provides a prediction

for the temporal window of the functional contribution of sensory responses in SNr to behaviour. Importantly, sensory responses could either promote or suppress movements, depending on their relative timing to the motor signal, providing a highly flexible means to integrate sensory and motor signals in nigrothalamic circuits.

Effects of deep brain stimulation

In our model correlated basal ganglia activity increased the number of rebound spikes in thalamocortical neurons. In particular, higher-order correlations lead to pauses in the SNr population activity promoting rebound spikes, while pairwise correlations alone did not affect the nigrothalamic transmission of motor signals (Figure 2B). This suggests that in Parkinson's disease higher-order correlations are relevant for motor symptoms, which offers some insight into the potential mechanisms by which deep-brain stimulation (DBS) might alleviate some of the motor symptoms such as rigidity and tremor. DBS in the STN and GPi has complex and diverse effects on the firing rate of neurons in SNr/GPi (Bar-Gad et al., 2004; Zimnik et al., 2015) and thalamus (Muralidharan et al., 2017). According to our model strong increases in SNr and GPi firing rates observed after STN DBS (Hashimoto et al., 2003; Maurice et al., 2003), would decrease the duration of the spontaneous pauses in the population activity (Figure 3C). Thereby, even for correlated SNr activity, the duration of the pauses would not be long enough to allow the generation of a rebound spike in the thalamocortical neuron. This conclusion also holds when a subset of neurons in SNr and GPi decrease their firing rate during STN DBS (Hahn et al., 2008; Humphries and Gurney, 2012). The decrease in the firing rate would decrease the degree of

566 correlation by eliminating or displacing the synchronous spike times and therefore weaken the
567 inhibition preceding the pauses that could have potentially evoked rebound spikes.

568 *Integration of decision making systems*

569 In our model the generation of a rebound spike in thalamocortical neurons was strongly affected
570 by single excitatory cortical input spikes (Figure 5). This means that the transmission of a basal
571 ganglia motor signal could be prevented by a single, precisely-timed cortical spike preceding
572 the SNr movement-related decrease by up to 20 ms (Figure 5C). This indicates a powerful
573 mechanism by which cortex could affect basal ganglia motor output signals. It has previously
574 been argued that different decision making systems, incorporating different strategies, might
575 co-exist in the brain (Redgrave et al., 1999; Daw et al., 2005) and that the thalamus might be a key
576 site for their integration (Haber and Calzavara, 2009). Our model offers a potential mechanism
577 by which conflicts between different decision-making systems could be resolved. In this case
578 the precisely-timed cortical excitation would allow the cancellation of a basal ganglia motor
579 signal. Furthermore, it is possible that thalamocortical neurons integrate habitual and goal-directed
580 decision systems (Daw et al., 2005; Redgrave et al., 2010), and that cancellation of basal ganglia
581 motor signals serves as a means to prevent conflicting responses. Finally, the same mechanism for
582 cancelling basal ganglia motor signals could also be used to exert cognitive control to overcome
583 a habitual response. While this remains speculative at this point, our model provides a clear
584 description of the inhibitory and excitatory inputs that would enable the modulation of a basal
585 ganglia motor signal in thalamocortical neurons.

Acknowledgements

This work was supported by Erasmus Mundus joint PhD program (EuroSPIN), the BrainLinks-BrainTools Cluster of Excellence funded by the German Research Foundation (DFG, grant number: EXC 1086), the EU H2020 Programme as part of the Human Brain Project (HBP-SGA1, 720270; HBP-SGA2, 785907), and the University of Sheffield. We also acknowledge support by the state of Baden-Wuerttemberg through bwHPC and the German Research Foundation (DFG) through grant no INST 39/963-1 FUGG. We would like to thank David Bilkey, Alejandro Jimenez, Lars Hunger, Amin Mirzaei, and Genela Morris for helpful discussions.

Competing Interests

The authors declare no competing financial interests.

Author Contributions

Mohammadreza Mohagheghi Nejad and Robert Schmidt designed the research. Robert Schmidt supervised the work. Mohammadreza Mohagheghi Nejad performed the simulations and analysed the data. Mohammadreza Mohagheghi Nejad, Stefan Rotter and Robert Schmidt interpreted the results and wrote the manuscript.

601 # References

603 Albin RL, Young AB, Penney JB (1989) The functional anatomy of basal ganglia disorders.
602
604 *Trends in neurosciences* 12:366–375.

605 Alexander GE, Crutcher MD (1990a) Functional architecture of basal ganglia circuits: neural
606 substrates of parallel processing. *Trends in neurosciences* 13:266–271.

607 Alexander GE, Crutcher MD (1990b) Neural representations of the target (goal) of visually guided
608 arm movements in three motor areas of the monkey. *Journal of neurophysiology* 64:164–178.

609 Avila I, Parr-Brownlie LC, Brazhnik E, Castañeda E, Bergstrom DA, Walters JR (2010) Beta
610 frequency synchronization in basal ganglia output during rest and walk in a hemiparkinsonian rat.
611 *Experimental neurology* 221:307–319.

612 Bar-Gad I, Elias S, Vaadia E, Bergman H (2004) Complex locking rather than complete
613 cessation of neuronal activity in the globus pallidus of a 1-methyl-4-phenyl-1, 2, 3,
614 6-tetrahydropyridine-treated primate in response to pallidal microstimulation. *Journal of*
615 *Neuroscience* 24:7410–7419.

616 Bar-Gad I, Heimer G, Ritov Y, Bergman H (2003) Functional correlations between
617 neighboring neurons in the primate globus pallidus are weak or nonexistent. *Journal of*
618 *Neuroscience* 23:4012–4016.

619 Bergman H, Feingold A, Nini A, Raz A, Slovin H, Abeles M, Vaadia E (1998) Physiological
620 aspects of information processing in the basal ganglia of normal and parkinsonian primates.
621 *Trends in neurosciences* 21:32–38.

622 Bosch-Bouju C, Hyland BI, Parr-Brownlie LC (2013) Motor thalamus integration of cortical,
623 cerebellar and basal ganglia information: implications for normal and parkinsonian conditions.
624 *Frontiers in computational neuroscience* 7:163.

625 Bosch-Bouju C, Smither RA, Hyland BI, Parr-Brownlie LC (2014) Reduced reach-related
626 modulation of motor thalamus neural activity in a rat model of parkinson's disease. *Journal*
627 *of Neuroscience* 34:15836–15850.

628 Brown P, Oliviero A, Mazzone P, Insola A, Tonali P, Di Lazzaro V (2001) Dopamine dependency
629 of oscillations between subthalamic nucleus and pallidum in parkinson's disease. *Journal of*
630 *Neuroscience* 21:1033–1038.

631 Bujan AF, Aertsen A, Kumar A (2015) Role of input correlations in shaping the variability and
632 noise correlations of evoked activity in the neocortex. *Journal of Neuroscience* 35:8611–8625.

633 Daw ND, Niv Y, Dayan P (2005) Uncertainty-based competition between prefrontal and
634 dorsolateral striatal systems for behavioral control. *Nature neuroscience* 8:1704.

635 Deniau J, Chevalier G (1985) Disinhibition as a basic process in the expression of striatal
636 functions. ii. the striato-nigral influence on thalamocortical cells of the ventromedial thalamic
637 nucleus. *Brain research* 334:227–233.

638 Edgerton JR, Jaeger D (2014) Optogenetic activation of nigral inhibitory inputs to motor thalamus
639 in the mouse reveals classic inhibition with little potential for rebound activation. *Frontiers in*
640 *Cellular Neuroscience* 8:36.

641 Ermentrout GB, Terman DH (2010) *Mathematical foundations of neuroscience*, Vol. 35 Springer
642 Science & Business Media.

643 Gaidica M, Hurst A, Cyr C, Leventhal DK (2018) Distinct populations of motor thalamic neurons
644 encode action initiation, action selection, and movement vigor. *Journal of Neuroscience* .

645 Gerstner W, Kistler WM (2002) *Spiking neuron models: Single neurons, populations, plasticity*
646 Cambridge university press.

647 Goldberg JH, Farries MA, Fee MS (2012) Integration of cortical and pallidal inputs in the basal
648 ganglia-recipient thalamus of singing birds. *Journal of neurophysiology* 108:1403–1429.

649 Goldberg JH, Farries MA, Fee MS (2013) Basal ganglia output to the thalamus: still a paradox.
650 *Trends in neurosciences* 36:695–705.

651 Goldberg JH, Fee MS (2012) A cortical motor nucleus drives the basal ganglia-recipient thalamus
652 in singing birds. *Nature neuroscience* 15:620–627.

653 Guo Y, Rubin JE, McIntyre CC, Vitek JL, Terman D (2008) Thalamocortical relay fidelity
654 varies across subthalamic nucleus deep brain stimulation protocols in a data-driven computational
655 model. *Journal of neurophysiology* 99:1477–1492.

Haber SN, Calzavara R (2009) The cortico-basal ganglia integrative network: the role of the thalamus. *Brain research bulletin* 78:69–74.

Hahn PJ, Russo GS, Hashimoto T, Miocinovic S, Xu W, McIntyre CC, Vitek JL (2008) Pallidal burst activity during therapeutic deep brain stimulation. *Experimental neurology* 211:243–251.

Hashimoto T, Elder CM, Okun MS, Patrick SK, Vitek JL (2003) Stimulation of the subthalamic nucleus changes the firing pattern of pallidal neurons. *Journal of neuroscience* 23:1916–1923.

Herd MB, Brown AR, Lambert JJ, Belelli D (2013) Extrasynaptic gabaa receptors couple presynaptic activity to postsynaptic inhibition in the somatosensory thalamus. *Journal of Neuroscience* 33:14850–14868.

Hikosaka O, Takikawa Y, Kawagoe R (2000) Role of the basal ganglia in the control of purposive saccadic eye movements. *Physiological reviews* 80:953–978.

Hikosaka O, Wurtz RH (1983) Visual and oculomotor functions of monkey substantia nigra pars reticulata. iv. relation of substantia nigra to superior colliculus. *Journal of neurophysiology* 49:1285–1301.

Huguenard J, Prince D (1994) Intrathalamic rhythmicity studied in vitro: nominal t-current modulation causes robust antioscillatory effects. *Journal of Neuroscience* 14:5485–5502.

Humphries MD, Gurney K (2012) Network effects of subthalamic deep brain stimulation drive a unique mixture of responses in basal ganglia output. *European journal of neuroscience* 36:2240–2251.

675 Kase D, Uta D, Ishihara H, Imoto K (2015) Inhibitory synaptic transmission from the substantia
676 nigra pars reticulata to the ventral medial thalamus in mice. *Neuroscience research* 97:26–35.

677 Kim J, Kim Y, Nakajima R, Shin A, Jeong M, Park AH, Jeong Y, Jo S, Yang S, Park H
678 et al. (2017) Inhibitory basal ganglia inputs induce excitatory motor signals in the thalamus.
679 *Neuron* 95:1181–1196.

680 Kojima S, Doupe AJ (2009) Activity propagation in an avian basal ganglia-thalamocortical circuit
681 essential for vocal learning. *Journal of Neuroscience* 29:4782–4793.

682 Kuhn A, Aertsen A, Rotter S (2003) Higher-order statistics of input ensembles and the response
683 of simple model neurons. *Neural Computation* 15:67–101.

684 Laudes T, Meis S, Munsch T, Lessmann V (2012) Impaired transmission at corticothalamic
685 excitatory inputs and intrathalamic gabaergic synapses in the ventrobasal thalamus of
686 heterozygous bdnf knockout mice. *Neuroscience* 222:215–227.

687 Leblois A, Bodor ÁL, Person AL, Perkel DJ (2009) Millisecond timescale disinhibition
688 mediates fast information transmission through an avian basal ganglia loop. *Journal of*
689 *Neuroscience* 29:15420–15433.

690 Leblois A, Meissner W, Bezard E, Bioulac B, Gross CE, Boraud T (2006) Temporal and spatial
691 alterations in gpi neuronal encoding might contribute to slow down movement in parkinsonian
692 monkeys. *European Journal of Neuroscience* 24:1201–1208.

693 Leblois A, Meissner W, Bioulac B, Gross CE, Hansel D, Boraud T (2007) Late emergence of
694 synchronized oscillatory activity in the pallidum during progressive parkinsonism. *European*
695 *Journal of Neuroscience* 26:1701–1713.

696 Lindahl M, Kotaleski JH (2016) Untangling basal ganglia network dynamics and
697 function–role of dopamine depletion and inhibition investigated in a spiking network model.
698 *eneuro* pp. ENEURO–0156.

699 Llinás R, Jahnsen H (1982) Electrophysiology of mammalian thalamic neurones in vitro.
700 *Nature* 297:406.

701 Magnin M, Morel A, Jeanmonod D (2000) Single-unit analysis of the pallidum, thalamus and
702 subthalamic nucleus in parkinsonian patients. *Neuroscience* 96:549–564.

703 Mallet N, Schmidt R, Leventhal D, Chen F, Amer N, Boraud T, Berke JD (2016) Arkypallidal
704 cells send a stop signal to striatum. *Neuron* 89:308–316.

705 Maurice N, Thierry AM, Glowinski J, Deniau JM (2003) Spontaneous and evoked activity of
706 substantia nigra pars reticulata neurons during high-frequency stimulation of the subthalamic
707 nucleus. *Journal of Neuroscience* 23:9929–9936.

708 Mirzaei A, Kumar A, Leventhal D, Mallet N, Aertsen A, Berke J, Schmidt R (2017) Sensorimotor
709 processing in the basal ganglia leads to transient beta oscillations during behavior. *Journal of*
710 *Neuroscience* 37:1289–17.

711 Muralidharan A, Zhang J, Ghosh D, Johnson MD, Baker KB, Vitek JL (2017) Modulation of
712 neuronal activity in the motor thalamus during gpi-dbs in the mptp nonhuman primate model of
713 parkinson's disease. *Brain stimulation* 10:126–138.

714 Nevado-Holgado AJ, Mallet N, Magill PJ, Bogacz R (2014) Effective connectivity of the
715 subthalamic nucleus–globus pallidus network during parkinsonian oscillations. *The Journal of*
716 *physiology* 592:1429–1455.

717 Pan WX, Brown J, Dudman JT (2013) Neural signals of extinction in the inhibitory microcircuit
718 of the ventral midbrain. *Nature neuroscience* 16:71.

719 Person AL, Perkel DJ (2005) Unitary ipsps drive precise thalamic spiking in a circuit required for
720 learning. *Neuron* 46:129–140.

721 Person AL, Perkel DJ (2007) Pallidal neuron activity increases during sensory relay through
722 thalamus in a songbird circuit essential for learning. *Journal of Neuroscience* 27:8687–8698.

723 Redgrave P, Prescott TJ, Gurney K (1999) The basal ganglia: a vertebrate solution to the selection
724 problem? *Neuroscience* 89:1009–1023.

725 Redgrave P, Rodriguez M, Smith Y, Rodriguez-Oroz MC, Lehericy S, Bergman H, Agid Y,
726 DeLong MR, Obeso JA (2010) Goal-directed and habitual control in the basal ganglia:
727 implications for parkinson's disease. *Nature Reviews Neuroscience* 11:760.

728 Reitsma P, Doiron B, Rubin JE (2011) Correlation transfer from basal ganglia to thalamus in
729 parkinson's disease. *Frontiers in computational neuroscience* 5:58.

730 Rinzel J (1985a) Excitation dynamics: insights from simplified membrane models In *Fed. Proc*,
731 Vol. 44, pp. 2944–2946.

732 Rinzel J (1985b) Excitation dynamics: insights from simplified membrane models In *Fed. Proc*,
733 Vol. 44, pp. 2944–2946.

734 Rubin JE, Terman D (2004) High frequency stimulation of the subthalamic nucleus eliminates
735 pathological thalamic rhythmicity in a computational model. *Journal of computational*
736 *neuroscience* 16:211–235.

737 Saito Y, Isa T (1999) Electrophysiological and morphological properties of neurons in the rat
738 superior colliculus. i. neurons in the intermediate layer. *Journal of neurophysiology* 82:754–767.

739 Schmidt R, Berke JD (2017) A pause-then-cancel model of stopping: evidence from basal ganglia
740 neurophysiology. *Phil. Trans. R. Soc. B* 372:20160202.

741 Schmidt R, Leventhal DK, Mallet N, Chen F, Berke JD (2013) Canceling actions involves a race
742 between basal ganglia pathways. *Nature neuroscience* 16:1118.

743 Schultz W (1986) Activity of pars reticulata neurons of monkey substantia nigra in relation to
744 motor, sensory, and complex events. *Journal of Neurophysiology* 55:660–677.

745 Staude B, Grün S, Rotter S (2010) Higher-order correlations and cumulants In *Analysis of parallel*
746 *spike trains*, pp. 253–280. Springer.

747 Ulrich D, Huguenard JR (1997) Nucleus-specific chloride homeostasis in rat thalamus. *Journal*
748 *of Neuroscience* 17:2348–2354.

749 Wichmann T, DeLong MR (1996) Functional and pathophysiological models of the basal ganglia.
750 *Current opinion in neurobiology* 6:751–758.

751 Wilson CJ (2013) Active decorrelation in the basal ganglia. *Neuroscience* 250:467–482.

752 Wilson CJ (2015) Oscillators and oscillations in the basal ganglia. *The Neuroscientist* 21:530–539.

753 Yin HH, Knowlton BJ (2006) The role of the basal ganglia in habit formation. *Nature Reviews*
754 *Neuroscience* 7:464.

755 Zimnik AJ, Nora GJ, Desmurget M, Turner RS (2015) Movement-related discharge in the
756 macaque globus pallidus during high-frequency stimulation of the subthalamic nucleus. *Journal*
757 *of Neuroscience* 35:3978–3989.